03,09

Effect of oxygen and carbon impurities on the parameters of a silicon cluster with a vacancy

© N.T. Sulaimanov[1], Sh.M. Makhkamov[1], M.Yu. Tashmetov[1], Sh.M. Nazarmamatov[1], S.R. Egamov[1], A.K. Rafikov[1], M.N. Erdonov[1], Kh.M. Kholmedov[2]

[1] Institute of Nuclear Physics, Uzbek Academy of Sciences, Tashkent, Uzbekistan
[2] Tashkent University of Information Technologies named after Muhammad al-Khwarizmi, Tashkent, Uzbekistan

E-mail: nadimbeksulaymanov@gmaile.com, muzaffarerdonov1978@yandex.ru

Received July 11, 2024
Revised November 5, 2024
Accepted December 12, 2024

Computer-based simulation in the density functional method approximation was used to study the effect of a vacancy on the structure of $Si_{29}H_{36}$ and $Si_{87}H_{70}$ clusters modified by the introduction of O and C atoms. It is shown that the O_i-Si-C_i complex is formed in a vacancy-free cluster with simultaneous introduction of C and O atoms, and $3H + C_i$ +Si and Si-O-V type complexes are formed in clusters with a vacancy. It was determined that carbon and oxygen positions depended to a greater extent on the size of a nanocluster, while oxygen in the $Si_{80}Si_{70}$ clusters interacted with the vacancy to form an *A*-center. It was found that deep levels might be caused by variation of the silicon cluster electron states due to the interaction between background impurities and a vacancy in the silicon cluster lattice cell. It was established that simultaneously introduced O and C atoms, depending on the nanocluster size and if interstitial silicon and hydrogen atoms were present, gave rise to formation of weakly interacting defective complexes and hydrogen atom migration into the nanocluster.

Keywords: silicon, nanocluster, defect, vacancy, process impurities, computer-based simulation, structure, lattice, ab initio calculation methods, energy levels, band gap.

DOI: 10.61011/PSS.2025.02.60671.187

1. Introduction

Wide use of single crystal silicon in modern solid-state electronic technology puts new requirements for crystal structure uniformity and purity. The presence of uncontrolled process and background impurities as well as structural intrinsic point defects even in small concentrations in semiconductor crystals may result in formation of miscellaneous complexes both on the master slice surface and in the matrix [1–3]. Physical mechanism and free system energy variation during cluster formation in a semiconductor lattice, the effect of surface, content of interstitial atoms of the base substance, cluster size and other factors on cluster formation patterns and applicability in semiconductor electronic devices are addressed in [4]. Study of the electronic structure of silicon oxide containing silicon clusters in [5] showed that the absence of a gap on top of the valence band of tetrahedral silicon modifications was attributable to filling by hydrogen states that were caused by saturation of loose bonds with hydrogen atoms at the cluster boundary. It was noted that the electronic structure of defect states in SiO_2 was defined primarily by the kind of atoms involved in chemical bond formation in low-dimensional systems. Aspects of silicon nanocluster formation in bulk silicon monoxide in thermal annealing are studied in [6]. During heat treatment of disproportionation three-phase silicon monoxide at temperatures from 800 to 1200 °C, the authors found that nanocrystalline silicon precipitates were formed in the amorphous SiO_x suboxide environment and the numbers of silicon crystallization centers varied non-monotonously depending on the annealing temperature. Experimental data of O and C effect on generation of microdefects in the form interstitial Si atom clusters during crystal growth is given in [7]. The authors found that the density of microdefects serving as nuclei for oxidation-induced stacking faults in boron-doped silicon single crystals increases with increasing O/C concentration ratio in the single crystal. Formation of small clusters containing 29 Si atoms during laser treatment [8] and ultradisperse nanoclusters $1 \div 5$ nm in diameter was found in [9] during ion implantation of silicon. Configuration space along the corresponding reactions and migration paths including formation and dissociation of interstitial carbon and oxygen complexes, C_iO_i and C_iO_{2i}, in silicon was studied ab initio in [10] It was established that formation/dissociation mechanisms took place through trapping/emission of mobile C_i impurities by O complexes fixed in the lattice.

One of such low-dimensional structural formations in silicon are clusters, formation of which can affect crystal properties considerably while keeping the phase state of the substance unchanged.

A combination of the nontraditional strong coupling and molecular dynamics methods was used in [11] to calculate the structure and electron states of silicon clusters with

29 Si atoms in the presence of carbon atoms and to show that carbon forms in silicon clusters a bridge bond with two Si atoms and is in a hexagonal position in the center of a cell forming the $Si_{29}H_{36}:C_i$ type defect.

However, according to the given data, variation of structural parameters and state of nanoclusters depends on their impurity composition and nanocluster size. Their variations in the presence of various defect states in the cluster can be forecasted using computer-based structure simulation methods [12].

The objective of this study is to examine the structural parameters, dimensions and main energy properties of $Si_{29}H_{36}$ and $Si_{80}Si_{70}$ nanoclusters containing background oxygen and carbon impurity atoms with participation of a vacancy in the cluster using the computer-based simulation method.

2. Method of calculating nanocluster model parameters

The computer-based method used to simulate the structure and electrophysical parameters of nanoclusters involves Chem 3d 16.0 multiparticle interconnected system visualization software, ORCA software package for ab initio calculation of structural and electrophysical parameters and energy spectra, Molecular Orbital Calculations energy property visualization and analysis software, and some theoretical assumptions used by the authors on the basis of [13–18]. ORCA (Optimization Rationalized Calculations Approximations by ab initio methods) multipurpose quantum-chemical calculation software package supporting the modern electronic structure calculation methods, including density functional theory (DFT), many-body perturbation theory and related cluster methods developed in 1999 was developed to ensure versatility, extendibility, high computational efficiency and user-friendliness, is provided at no charge for academic users [13]. ORCA uses standard Gaussian basis functions and features full computation parallelization.

To detect physical processes that take place during formation of quantum dots and exposure to impurity atoms, the existing theoretical calculations in silicon nanocrystals are based mainly on two approaches: multiband effective mass method involving electrons and holes, and strong coupling method for simulation radiative and nonradiative processes in nanostructures. These methods consider the interactions of an atom with the nearest matrix atoms, and participation of related atoms or doping impurities in nanocluster formation and properties is not addressed. Ab initio theoretical calculations of physical properties in computer-based simulation of systems consisting of N_x particles imply dynamic change of electronic gas in a field of slowly varying atomic nucleus parameters.

As it is unrealistic to consider all interactions between all electrons and atoms, various approaches are generally used in practice to simplify the equation of state, however, the requirement for maximum possible reproduction of structure and energy parameters of a real multiparticle system shall be kept unchanged. From this standpoint, the density functional theory (DFT) method is the most informative for description of the equilibrium energy state of an electronic structure and properties of an interacting many-particle system, including semiconductor atom clusters. DFT method describes the full energy of a cluster system by equations [14]

$$E_{DFT}[\rho] = T_S[\rho] + E_{ne}[\rho] + J[\rho] + E_{XC}[\rho] \qquad (1)$$

where $T_S[\rho]$ is the kinetic energy of all electrons; $E_{ne}[\rho]$ is the electron-nucleus attraction energy and $J[\rho]$ is the Coulomb electron repulsion energy in an interconnected particle system; $E_{XC}[\rho]$ is the exchange-correlation interaction energy functionality.

All functionalities are functions of electron state densities ρ. Exchange-correlation interaction energy is calculated as follows

$$E_{XC}[\rho] = T[\rho] + T_S[\rho] - E_{ee}[\rho] - J[\rho] \qquad (2)$$

where $T[\rho]$ is the kinetic energy of a particle system; $E_{ee}[\rho]$ is the interaction energy of electrons involved in binding in the system.

If a functionality was found in the DFT method, calculations are performed identically to the quantum mechanics: a set of orthogonal orbitals is determined by the energy minimization method. Advantage of the DFT method: only the full electron density shall be calculated in the base energy state of an interconnected particle system. Therefore, a known set of ab initio methods was used to simulate the structure and properties of multiparticle systems — ORCA in a local electron density state approximation (DFT-LDA) (1-st order density functional theory approximation), where the electron state in homogeneity is considered. Selection of a basic set of atomic orbitals is an important aspect affecting the accuracy. If the selection is correct, then optimization calculations will be performed with a proper accuracy both for structural and energy parameters. The calculations used the atomic orbital basis set 6-31 G** where polarization along all atoms was considered and core electron simulation was improved [14]. It is considered to be the best rate-accuracy trade-off and is most widely used, but it is not available for elements from H to Kr. Then a nonpolarized set of double exponents (DZ) of Slater type nonpolarized basis functions was used in the approximated DFT calculations by the BLYP method [15].

Besides the full electron basis set, this method also addresses a set with a frozen nucleus approximation, which allows the calculation algorithm efficiency to be improved by reducing the basis size. Such approach makes it possible to apply additional approximation def2/J, as described in [16], to the density functional theory. Calculations of hydrogen-passivated doped silicon clusters use the following minimum basis sets for Si: $16s10p1d$ giving rise to$4s3p1d$ in the form of {6631/631/1}; for H — $4s1p$ giving rise to $2s1p$ in the

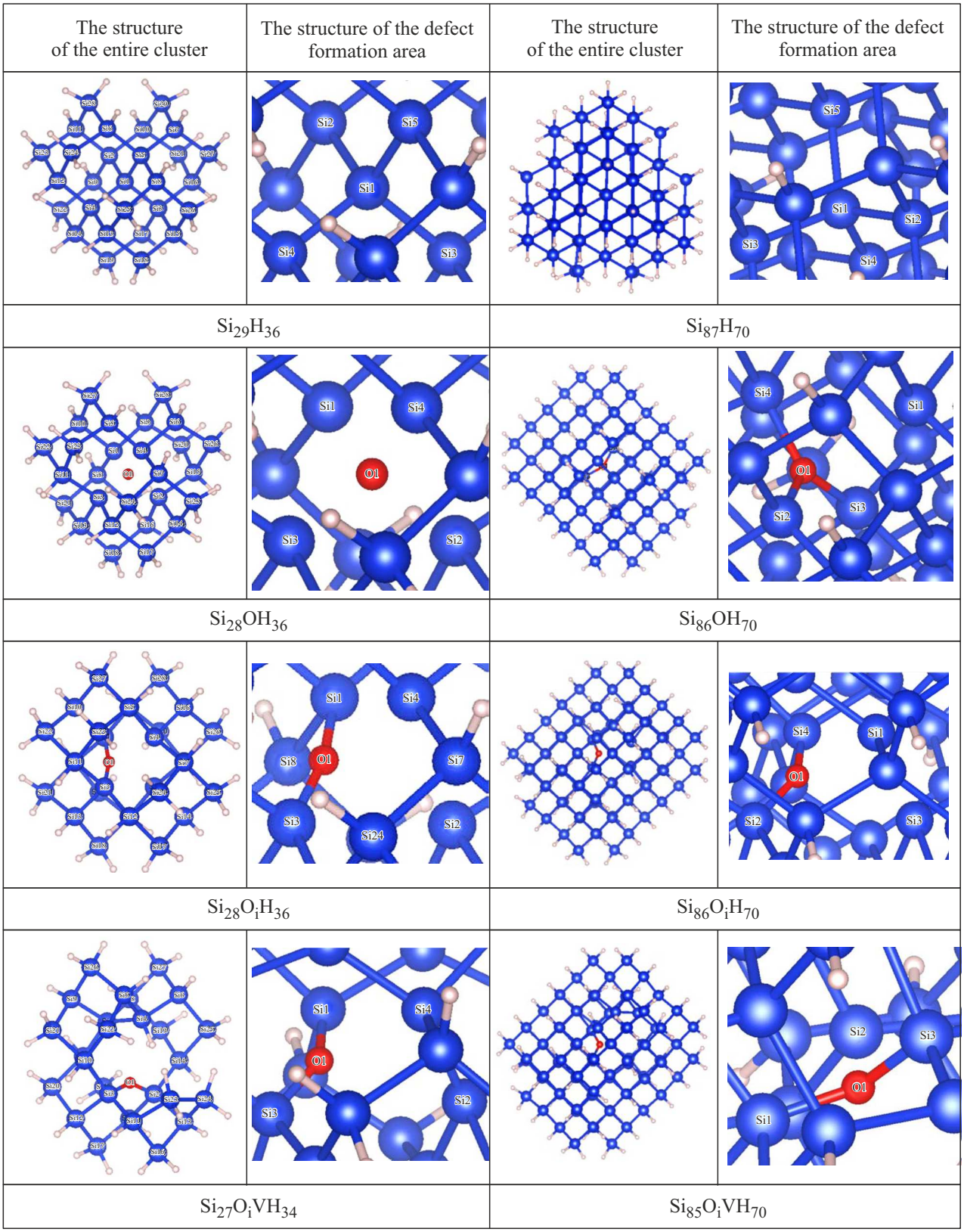

Figure 1. Structures of optimized $Si_{29}H_{36}$, $Si_{80}Si_{70}$ clusters and their derivatives during vacancy formation and introduction of O atom (columns 1 and 3); intrinsic and impurity defect formation areas are scaled-up (columns 2 and 4).

Table 1. Symmetry group, nanocluster diameters and radii of local defect areas in nanoclusters

Nanoclusters	G_s	D (Å)	R_1 (Å)	Nanoclusters	G_s	D (Å)	R_1 (Å)
$Si_{29}H_{36}$	T_d	10.672	2.384	$Si_{87}Si_{70}$	T_d	17.832	2.400
$Si_{28}OH_{36}$	C_∞	10.583	2.097	$Si_{86}OH_{70}$	C_∞	17.974	1.950
$Si_{28}O_iH_{36}$	C_{2v}	10.612	2.097	$Si_{86}O_iH_{70}$	C_{2v}	18.238	1.736
$Si_{27}O_iVH_{34}$	C_4	11.861	1.698	$Si_{85}O_iVH_{70}$	C_4	17.885	1.749
$Si_{28}CH_{36}$	C_∞	10.578	1.982	$Si_{86}CH_{70}$	T_d	17.902	2.401
$Si_{27}C_iVH_{34}$	T_d	10.709	1.974	$Si_{86}C_iH_{70}$	C_{4v}	17.941	2.054
				$Si_{85}C_iVH_{70}$	C_4	17.712	1.903
$Si_{28}O_sC_iH_{36}$	C_{4h}	11.106	1.409	$Si_{87}C_iO_iH_{70}$	C_{4v}	17.974	0.408
$Si_{28}VO_iC_iH_{36}$	$> C_s$	11.471	0.766 1.257*	$Si_{86}VC_iO_iH_{70}$	$> C_s$	17.953	2.141; 2.183

Note: D is the nanocluster diameter; G_s is the symmetry group in the local defect formation area R_1 is the distance between the atom (or vacancy) in the nanocluster center with the 1-st adjacent atoms; * — $R_{V\text{-}H}$ — is the distance between the vacancy and hydrogen atom migrated from outside the cell.

form of $\{31/1\}$; for P — $16s10p1d$ giving rise to $4s3p1d$ in the form of $\{6631/631/1\}$; for B — $10s4p1d$ giving rise to $3s2p1d$ in the form of $\{631/31/1\}$.

Moreover, the BLYP method includes the dependences of exchange and correlation energy not only from the electron density, but also from density derivatives. Similar methods are known as gradient correction methods or generalized gradient approximations (GGA) [16,17]. Most of them are associated with the functional modification LSDA (local spin density approximations). In the BLYP method, the exchange-correlation energy with gradient is written as

$$E_{XC}^{GGA}[n_\downarrow n_\uparrow] = \int d\vec{r}\ f\left(n_\uparrow(\vec{r}), n_\downarrow(\vec{r}), \Delta n_\uparrow(\vec{r}), \Delta n_\downarrow(\vec{r})\right) \tag{3}$$

where $n_\uparrow(\vec{r})$ and $n_\downarrow(\vec{r})$ — concentrations of spin-up and spin-down electrons, respectively, $\Delta n_\uparrow(\vec{r})$ and $\Delta n_\downarrow(\vec{r})$ are concentration variations in interaction.

Exact analytical expression for $f(n_\uparrow(\vec{r}), n_\downarrow(\vec{r}), \Delta n_\uparrow(\vec{r}), \Delta n_\downarrow(\vec{r})$ was obtained in the integral form in [17]. But due to the difficulty in using the integral form in the BLYP approximation, an exchange-correlation potential equation derived in [18] was used herein.

$$V_{XC}[n(\vec{r})] = \frac{\partial E_{XC}[n]}{\partial n(\vec{r})} - \nabla \cdot \frac{\partial E_{XC}[n]}{\partial \nabla n(\vec{r})} \tag{4}$$

where $\frac{\partial E_{XC}[n]}{\partial n(\vec{r})}$ is the particular derivative of the exchange-correlation energy term with respect to the charge carrier density $n(\vec{r})$, $\nabla = \frac{\partial}{\partial r}$ is the differential operator, $\frac{\partial E_{XC}[n]}{\partial \nabla n(\vec{r})}$ is the particular derivative of the exchange-correlation energy term with respect to the rate of change of the charge carrier density $n(\vec{r})$.

Thus, to evaluate the influence of exchange-correlation functional, the BLYP gradient-corrected functionals (GGA) [15] and the B3LYP hybrid functional (hybrid means a combination of exchange contributions defined by the Hartree–Fock method, and DFT functionals) were chosen [17]. However, the B3LYP method increases the computation time considerably. To reduce the computer-based cluster modelling time, the BLYP method was used, as it was previously the case in [18].

3. Findings and discussion

3.1. Structural parameters of nanoclusters

A small-size Si cluster state may be controlled by varying the geometrical position and charge state of impurity atoms. Furthermore, in terms of an instrumental physical analysis, interaction of the introduced C and O atoms with theV_{Si} type intrinsic defect in the cluster is a very labour-intensive process. Therefore, optimization calculations of structural parameters and corresponding energy properties used the algorithms of approximation to the electron energy state density theory in a polyatomic interacting system within ORCA calculation program package, version 5 [13,18]. The calculated structural parameters are listed below in Tables 1 and 2, and the atomic structure of the silicon cluster with intrinsic and impurity defects is shown in Figure 1.

Optimized nanocluster geometries generally retain the sizes and symmetry, and formation of defects (Figures 1–3) decreases local area symmetries. In this case, the nanocluster geometry varies from spherical to slightly elongated ellipsoidal. When the main Si atom is substituted with impurity (O, C), the effect of the resultant defect area doesn't cover the whole nanocluster, and symmetry reduction ($T_d \to C$) doesn't lead to a drastic change of crystal system, except the interstitial O (Figure 1). Oxygen integrated into an interstitial site of the cluster lattice cell with a vacancy forms equilibrium bonds with Si atoms [19,20].

Table 2. Distances between the central Si atom (or V_{Si}) and impurity atoms in local defect areas of nanoclusters

Nanoclusters	R_2 (Å)	R_3 (Å)	Nanoclusters	R_2 (Å)	R_3 (Å)
$Si_{27}O_iVH_{34}$	1.26	1.71 2.07 2.41	$Si_{85}O_iVH_{70}$	0.829	1.749 1.752 3.209 4.180
$Si_{28}C_sH_{36}$	–	–	$Si_{86}C_sH_{70}$	–	–
			$Si_{86}C_iH_{70}$	–	–
$Si_{27}C_iVH_{34}$	0.104	1.935 1.966	$Si_{85}C_iVH_{70}$	0.577	2.042 2.076 2.081 4.564
$Si_{28}O_iC_sH_{36}$	1.414	2.469 2.883 2.854 2.962	$Si_{87}C_iO_iH_{70}$	1.405 1.705	0.408 2.076 2.953 2.218
$Si_{28}VO_iC_iH_{36}$	2.844	2.889 2.879 2.918 3.189	$Si_{86}VC_iO_iH_{70}$	1.426	2.141 2.183 2.199 2.664
$Si_{29}O_iC_sH_{36}$	1.414	2.469 2.883 2.854 2.962	$Si_{87}C_iO_iH_{70}$	1.405 1.705	0.408 2.076 2.953 2.218
$Si_{29}O_sC_iH_{36}$	1.428	0.978 2.765 2.771 2.959			
$Si_{28}VH_{36}$	–	2.111	$Si_{86}VH_{70}$	–	2.136 2.148 2.191 2.191 2.206
$Si_{28}VO_iC_iH_{36}$	2.844	2.889 2.879 2.918 3.189	$Si_{86}VC_iO_iH_{70}$	1.426	2.141 2.183 2.199 2.664

Note: R_2 are the distances between impurity atoms (O, C); R_3 are the distances between the vacancy in the central site of a lattice and the nearest Si atoms.

When O atom is introduced into the $Si_{29}H_{36}$ cluster lattice cell without a vacancy, then it doesn't form equilibrium covalent bonds with Si atoms at the end of the optimization cycle, but moves to the central site position: $Si_{29}H_{36} + O \rightarrow Si_{28}O_sH_{36}$, defect area symmetry group is C_{4v} (symmetry elements hereinafter correspond to the data of [20]).

If there is a vacancy in this area, O_i forms bonds with two nearest Si atoms, but, unlike a Si single crystal, an *A*-center is not formed in the nanocluster, the defect area symmetry group in this case is C_{2v}. Optimization of the $Si_{86}O_iH_{70}$ nanocluster model shows that the interstitial O position is more stable, i. e. formation of the *A*-center depends on the nanocluster size (Table 2):

$$Si_{28}VH_{36} + O_i \rightarrow Si_{26}[Si : O_i : Si]VH_{36}$$

$$Si_{86}VH_{36} + O_i \rightarrow Si_{86}[O_i : V]H_{70}.$$

Such change of symmetry around a point defect — from T_d to C_{2v} and strong dependence of electron state polarization on the interaction between V and interstitial O agree well with those for O in single crystal Si [19,21] and partially confirm the *ab initio* study data for Si nanoparticles with O defect [22]. But for the $Si_{28}VH_{36}$ cluster, agreement with data provided by other authors is not observed [19–22].

Review of the literature data [23,24] shows that an interstitial C atom in a Si lattice more likely occupies an interstitial site, and the authors of [25], based on the analysis of carbon-induced charged states and deep levels, suggested that C may occupy a lattice site in some cases. For $Si_{29}H_{24}$ and $Si_{29}H_{36}$ nanoclusters, equilibrium neutral and charged states of the interstitial C atom were examined in [11].

In the given optimized model of interstitial C atom in the interstitial site of the $Si_{29}H_{36}$ nanocluster, defect formation reaction is written as: $Si_{29}H_{36} + C_i \rightarrow Si_{28}CsH_{36}$, where C_s forms bonds with four Si atoms and occupies the central site. As the nanocluster size increases, probabilities of C presence in the main and interstitial sites will become equal, with the same symmetry groups (T_d) (Figure 2). Defect formation reaction is written as:

$$Si_{80}Si_{70} + C_i \rightarrow Si_{86}C_iH_{70} \equiv Si_{80}Si_{70} + C_s \rightarrow Si_{86}C_iH_{70}$$

When C atom is introduced into the lattice cell containing a vacancy, defect formation reactions may be written as:

$$Si_{28}VH_{36} + C_i \rightarrow Si_{28}C_sH_{36} \equiv Si_{28}VH_{36} + C_s \rightarrow Si_{28}C_sH_{36}$$

$$Si_{86}VH_{70} + C_i \rightarrow Si_{85}VC_iH_{70} \equiv Si_{86}VH_{70} + C_s \rightarrow Si_{85}VC_iH_{70}$$

Corresponding symmetry groups: T_d for $Si_{28}CsH_{36}$ and C_{4v} for $Si_{85}VC_iH_{70}$. As a result of cumulative effect of atoms in the $Si_{28}VH_{36}$ nanocluster, C atom occupies a vacant site ($C_i \rightarrow C_s$), and as a result of C atom introduction near the vacancy in the $Si_{86}VH_{70}$ nanocluster, the [3Si-C_i-V] defect complex is formed, which agrees well with the data provided by the authors of [10,26,27].

Comparative analysis of the optimized nanocluster geometries with impurity atoms shows that, regardless of the method and sequence of simultaneous introduction of O and C atoms into ultradisperse Si clusters, the O atom occupies an interstitial site, and the C atom occupies a lattice cell site (if there is a vacancy in the interstitial area) or moves to an interstitial site with formation of a defect complex {[Si-Ci-3H]. . . O_i} (Figure 3). Changes of symmetries in defect areas of nanoclusters in this case explicitly depend on dimensional effects. The formation of complex interstitial impurity atoms is also indicated in [28–30].

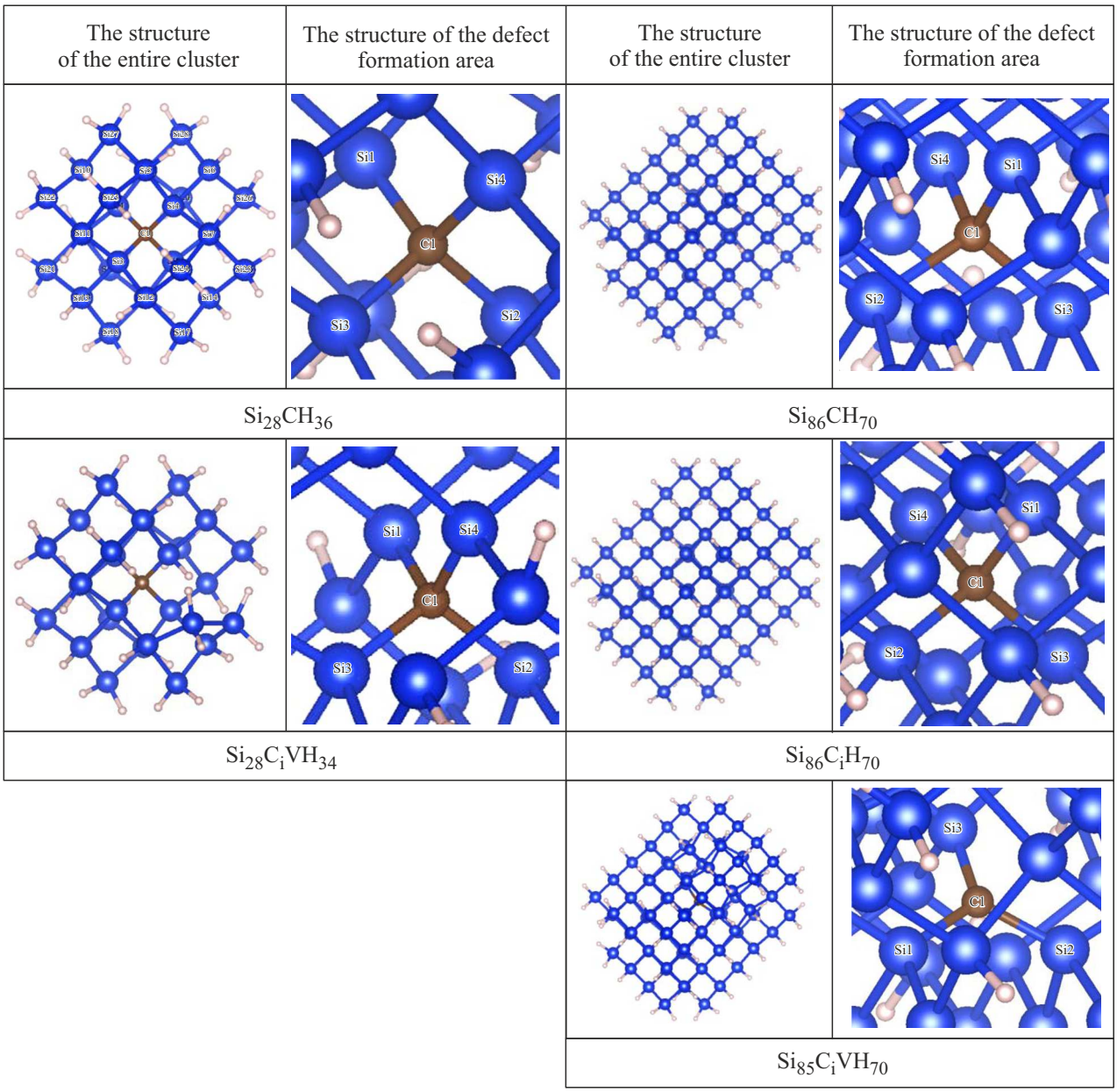

Figure 2. Structures of optimized $Si_{29}H_{36}$, $Si_{80}Si_{70}$ clusters and their derivatives during vacancy formation and introduction of C atom; intrinsic and impurity defect formation areas are scaled-up.

If the presence of H atoms in the Si cluster is considered, then, with reduction of the defect formation area symmetry and migration of H atoms, new defect complexes are formed:

$$Si_{29}H_{36} + O + C \rightarrow Si_{26}\{[Si\text{-}C_i\text{-}2H]\text{-}V\text{-}O_i\text{-}Si]\}H_{37}$$

$$Si_{29}H_{36} + C + O \rightarrow Si_{26}\{[Si\text{-}C_i\text{-}2H] + V\text{-}Si\text{-}O_i]\}H_{38}$$

Possibility of such H atom migration from the surface was proposed previously for the $Si_{10}H_{16}$ nanocluster in [30], where H atom introduction into the nanocluster is described by the Si–H bond dissociation model. Introduction of O and C atoms into a large $Si_{87}Si_{70}$ nanocluster leads to formation of the $[V_{Si} + Si_i]$ pair [20,25,28]. The following quasi chemical reactions with formation of complex structural defects take place in this case:

$$Si_{87}Si_{70} + C + O \rightarrow Si_{84}\{[V\text{-}Si_i] + [Si_i\text{-}C_i\text{-}Si] + [Si_i\text{-}O_i\text{-}Si]\}H_{70}$$

(C and O atoms are introduced in the same lattice cell)

$$Si_{87}Si_{70} + C + O \rightarrow Si_{84} \times \{[V\text{-}Si] + [C_i\text{-}3Si] + [O_i\text{-}2Si]\}H_{70}$$

(C and O atoms are introduced in neighboring lattice cells).

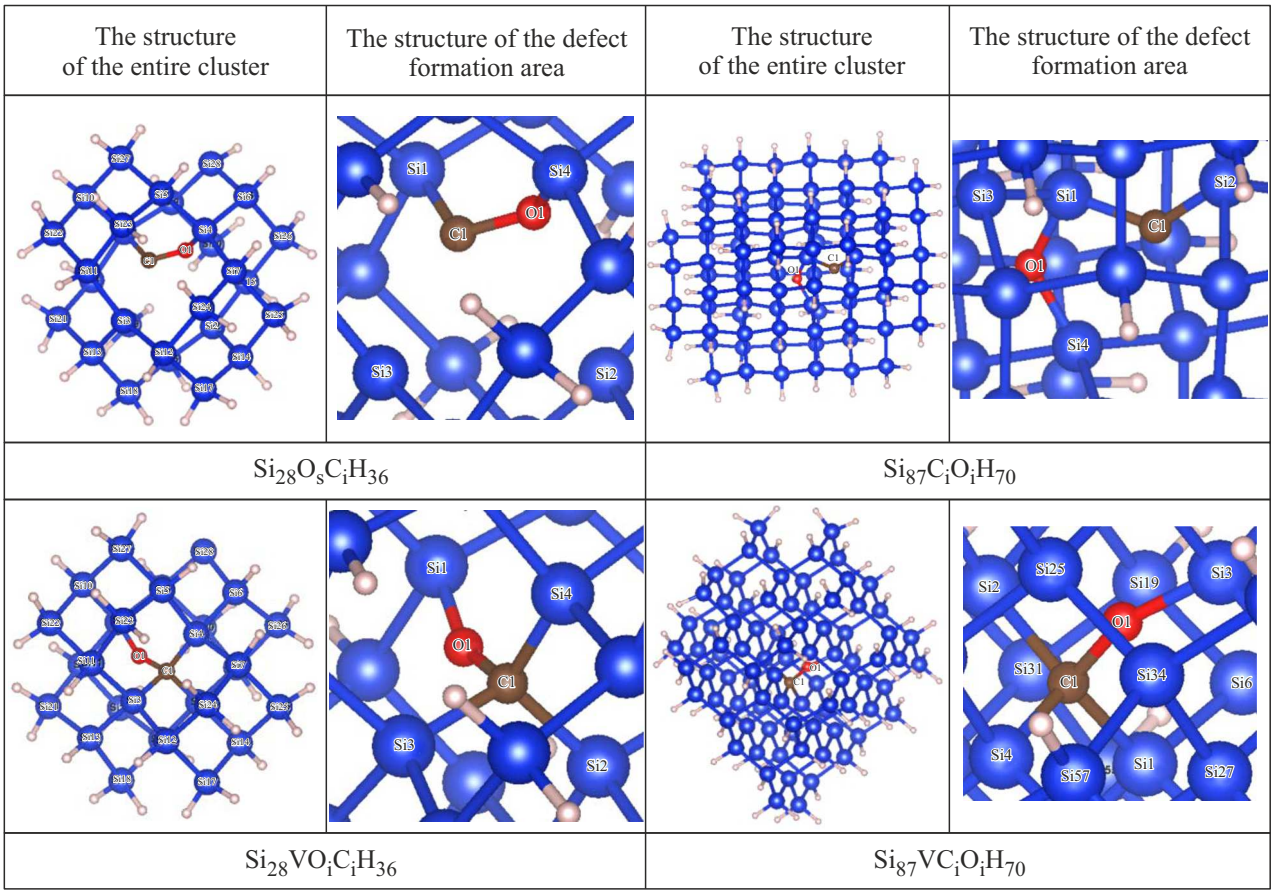

Figure 3. Structures of optimized $Si_{29}H_{36}$, $Si_{80}Si_{70}$ clusters and their derivatives during vacancy formation and introduction of O and C atoms; intrinsic and impurity defect formation areas are scaled-up.

Table 3. Main energy parameters of the $Si_{29}H_{36}$, $Si_{28}VH_{36}$, $Si_{87}H_{70}$, $Si_{86}VH_{70}$ nanoclusters and their derivatives formed by way of simultaneous introduction of impurity atoms (O, C)

Cluster	E_g (eV)	E_{pa} (eV)	D (Debay)	Cluster	E_g (eV)	E_{pa} (eV)	D (Debay)
$Si_{29}H_{36}$	−5.63	−8413	0.0002	$Si_{87}H_{70}$	−3.23	−25220	0.075
$Si_{28}VH_{36}$	−6.07	−8123	0.00016	$Si_{86}VH_{70}$	−3.06	−24931	0.09066
$Si_{28}OH_{36}$	−6.18	−8199	0.0006	$Si_{86}OH_{70}$	−3.21	−25006	3.089
$Si_{27}O_iVH_{34}$	−6.03	−7909	0.4366	$Si_{85}VO_iH_{70}$	−3.36	−24717	2.456
$Si_{28}CH_{36}$	−6.01	−8164	0.0003	$Si_{86}CiH_{70}$	−3.23	−24969	0.073
$Si_{27}CiVH_{34}$	−5.94	−7872	0.5737	$Si_{85}VCiH_{70}$	−3.31	−24679	1.722
$Si_{28}OsCiH_{36}$ (alpha)	−5.616	−8239	0.9468	$Si_{87}OiCiH_{70}$	−3.04	−25334	1.809
$Si_{28}OsCiH_{36}$ (beta)							
$Si_{28}OiCsH_{36}$	−5.575	−8239	0.6907				
$Si_{28}VOiCiH_{36}$	−5.535	−8237	0.4766	$Si_{86}VOiCiH_{70}$	−3.47	−25044	0.392

Note: E_g is the band gap width; E_{pa} is the bond energy per each atom in the nanocluster. D are nanocluster dipole moments.

$Si_{29}H_{36}$, $E_g = -5.6311$ eV,
$E_{c1} = -6.8760$ eV
$E_{v4} = -1.7376$ eV, $^2E_{v3} = -1.5536$ eV,
$^3E_{v2} = -1.4325$ eV, $E_{v1} = -1.2449$ ev
$E_{v1} = -0.4826$ eV.

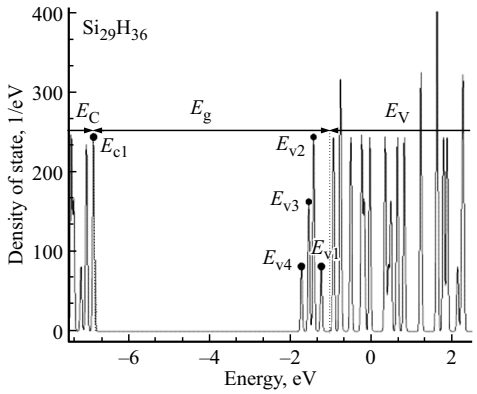

$Si_{28}VH_{36}$, $E_g = -6.0684$ eV,
$E_{c1} = -6.5510$ eV, $E_{v6} = -1.8470$ eV,
$^2E_{v5} = -1.7242$ eV, $E_{v4} = -1.4770$ eV,
$^2E_{v3} = -1.2215$ eV, $E_{v2} = -0.9383$ eV,

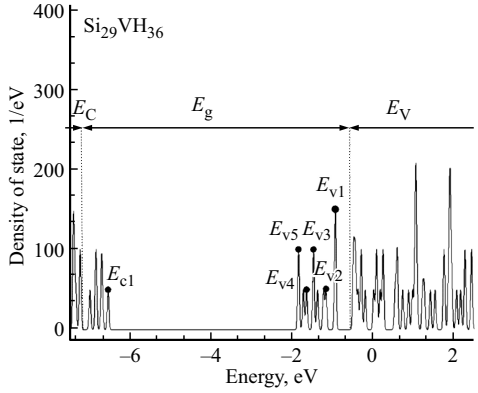

$Si_{28}OH_{36}$, $E_g = -6.1763$ eV,
$E_{c1} = -6.8992$ eV
$E_0 = -4.7131$ eV, $E_{v5} = -1.7038$ eV,
$E_{v4} = -1.5085$ eV, $E_{v3} = -1.1322$ eV,
$E_{v2} = -1.0712$ eV, $E_{v1} = -0.7229$ eV.

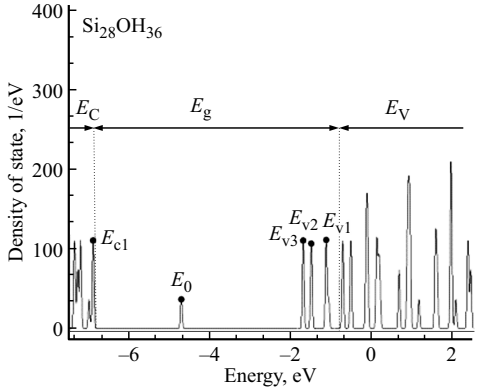

$Si_{28}VOH_{36}$, $E_g = -6.0276$ eV
$E_{c1} = -6.7200$ eV, $^3E_{v5} = -1.6986$ eV,
$^2E_{v4} = -1.4773$ eV, $^2E_{v3} = -1.2685$ eV,
$E_{v2} = -0.9643$ eV, $E_{v1} = -0.6924$ eV.

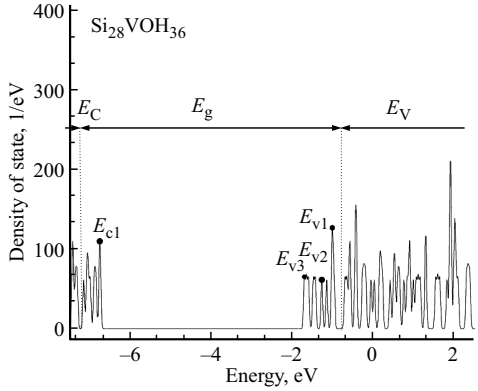

$Si_{28}C_sH_{36}$, $E_g = -6.0018$ eV,
$E_{c1} = -6.6812$ eV, $E_{v5} = -1.6259$ eV,
$E_{v4} = -1.5111$ eV, $E_{v3} = -1.1842$ eV,
$^2E_{v2} = -1.0736$ eV, $E_{v1} = -0.6794$ eV.

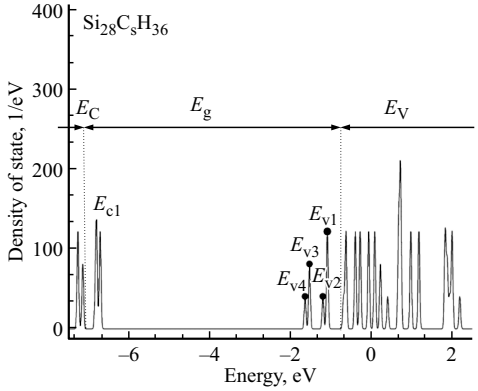

$Si_{27}VCH_{34}$, $E_g = -5.9415$ eV,
$E_{c1} = -6.7535$ eV, $E_{v5} = -1.7948$ eV,
$^2E_{v4} = -1.4627$ eV, $E_{v3} = -1.2063$ eV,
$E_{v2} = -1.0070$ eV, $E_{v1} = -0.8120$ eV.

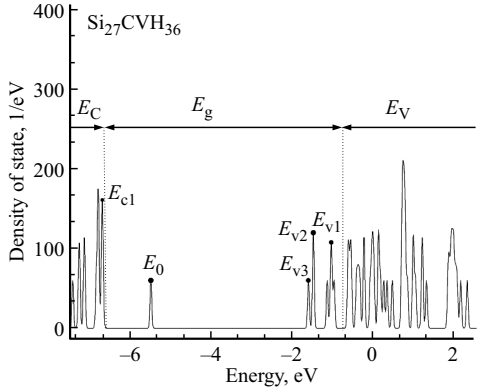

Figure 4. Energy parameters and dependences of electron energy levels on the densities of states of the $Si_{29}H_{36}$, $Si_{28}VH_{36}$ nanoclusters and their derivatives formed by the interstitial O or C atom separately. E_{c1} is the conduction band bottom; E_{v1} valence band ceiling; a degree indicates the energy level multiplicity, i. e. this is a degeneracy multiplicity. For example: $^3E_{v2} = -1.4325$ eV — level E_{v2} is triply degenerate.

$Si_{28}O_sC_iH_{36}$ (alpha), $E_g = -5.6161$ eV, $E_{c1} = -7.0679$ eV, $E_{c2} = -6.7813$ eV, $E_{v1} = -1.4518$ eV, $E_{v2} = -1.7311$ eV. $E_{0\alpha} = -5.4$ eV	$Si_{28}VO_iC_iH_{36}$, $E_g = -5.5355$ eV, $E_{v1} = -6.9656$ eV, $E_{v2} = -6.7725$ eV, $E_{v3} = -6.7568$ eV, $E_{v4} = -6.6221$ eV, $E_{c1} = -1.4301$ eV, $E_{c2} = -1.7971$ V.
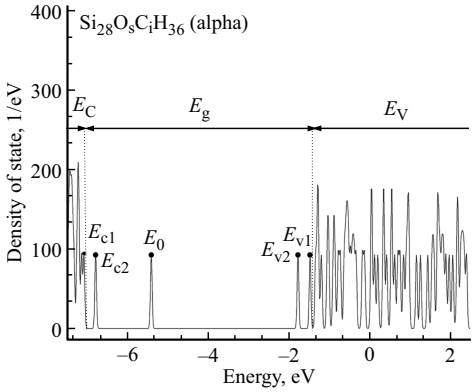	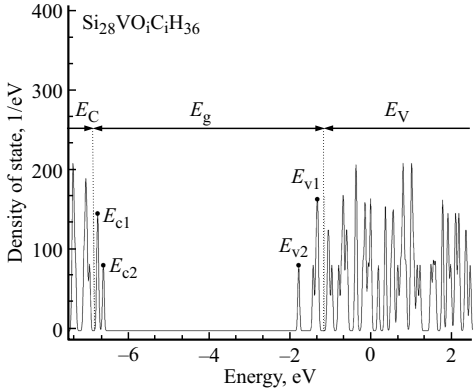
$Si_{28}O_sC_iH_{36}$ (beta), $E_g = -5.6161$ eV, $E_{c1} = -7.0679$ eV, $E_{c2} = -6.7813$ eV, $E_{v1} = -1.4518$ eV, $E_{v2} = -1.7311$ eV. $E_{0\beta} = -2.9418$ eV	$Si_{28}O_iC_sH_{36}$, $E_g = -5.5752$ eV, $E_{c1} = -7.0806$ eV, $E_{c2} = -6.7892$ eV, $E_{v1} = -1.5054$ eV, $E_{v2} = -1.8143$ eV.
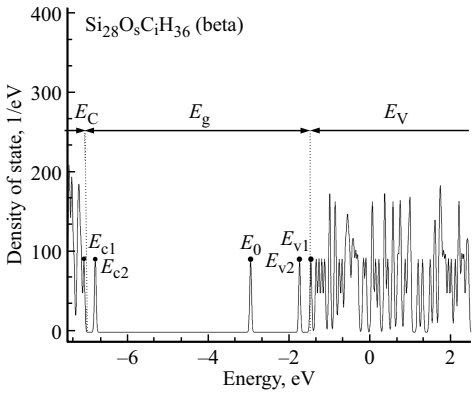	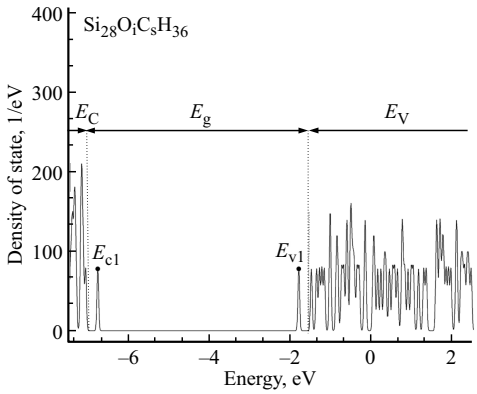
$Si_{87}Si_{70}$, $E_g = -3.0244$ eV. $E_{v1} = -5.5318$ eV, $E_{c1} = -2.5074$ eV. $E_{v5} = -5.4038$ eV, $E_{c2} = -2.5843$ eV, $E_{c3} = -2.5689$ eV, $E_{c4} = -2.5585$ eV,	$Si_{86}VH_{70}$, $E_g = -3.2652$ eV. $E_{v1} = -5.4050$ eV, $E_{c1} = -2.1398$ eV, $E_{v5} = -5.2035$ eV, $E_{c2} = -2.4713$ eV, $E_{c3} = -2.3543$ eV. $E_{01} = -3.5410$ eV, $E_{02} = -3.2766$ eV.
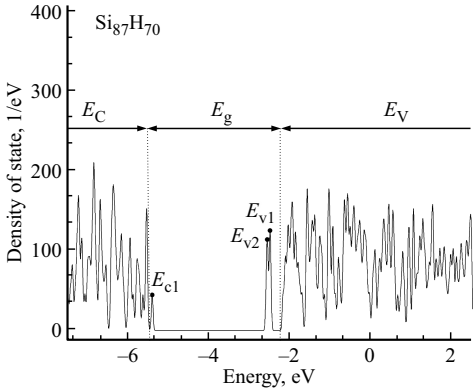	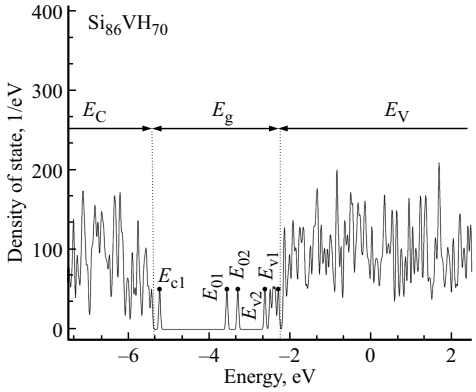

Figure 5. Energy parameters and dependences of energy levels on the densities of states of the $Si_{29}H_{36}$, $Si_{28}VH_{36}$ nanocluster and their derivatives formed through the simultaneous introduction of impurity atoms (O, C) E_{c1} is the conduction band bottom; E_{v1} is the valence band ceiling; a degree indicates the energy level multiplicity, i. e. this is the degeneracy multiplicity. For example: $^3E_{v2} = -1.4325$ eV — level E_{v2} is triply degenerate.

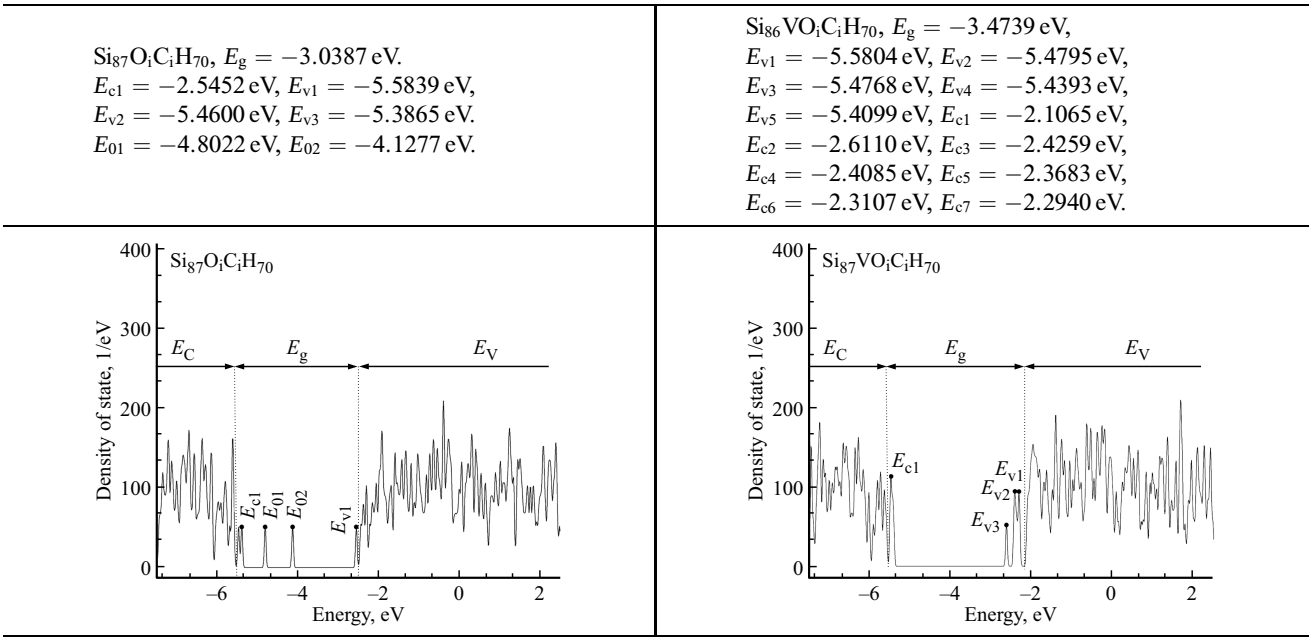

Figure 5 (*cond.*).

The following quasi chemical reactions are possible, if O and C atoms are introduced simultaneously in the nanoclusters ($Si_{28}VH_{36}$ and $Si_{86}VH_{70}$) with a vacancy in the central site:

$$Si_{28}VH_{36} + O + C \rightarrow Si_{27}[Si\text{-}C_i\text{-}3H] + [O_i\text{-}H\text{-}V]\}H_{38}$$

$$Si_{86}VH_{70} + O + C \rightarrow Si_{85}[C_i\text{-}V] + [C_i\text{-}O_i\text{-}Si]H_{69}$$

(C and O atoms are introduced in the same lattice cell)

$$Si_{86}VH_{70} + O + C \rightarrow Si_{83}\{[Si\text{-}V] + [C_i\text{-}O_i\text{-}2Si]\}H_{69}$$

(C and O atoms are introduced in the neighboring lattice cells) This means that the structure of the defect complex formation area containing the vacancy and impurity atom of the given nanoclusters depends not only on the relative positions of the impurity atoms and intrinsic defects, but also on the effects depending on the size (Frenkel pair, *A*-center formation mechanisms, Jahn-Teller effect) and on quantum phenomena [11,18,26].

Review of the obtained tabular data and calculated structural parameters of Si clusters containing impurity and vacancy defects showed that formation of defects in the cluster modifies the local area symmetries depending on the impurity position in the cluster and the Si nanocluster size. I. e. the O impurity in $Si_{28}OH_{36}$ causes an increase in the lattice parameter, and the C impurity in $Si_{28}CH_{36}$ causes a decrease in the lattice parameter. If there are C and O in the $Si_{28}OCH_{36}$ cluster, the defect formation area symmetry decreases sharply and the lattice parameter increases.

3.2. Nanocluster energy parameters and electron levels

To examine energy properties of nanoclusters with intrinsic, process and interstitial impurity defects, diagrams of electron distributions over energy levels vs. the densities of energy states in the cluster band gap were built (Figures 1 and 2). Nanocluster band gap widths are defined as the difference of E_{c1} and E_{v1}: $E_g = E_{c1} - E_{v1}$, where E_{c1} is the conduction band bottom, E_{v1} is the valence band ceiling. Calculations of energy properties and electron level spectrum show that small levels, multiples in most cases, are always formed in the nanocluster band gaps. Values of these and deep levels caused by the impurity atoms differ from the levels in a Si single crystal (Figure 4).

As shown in Figure 4, the interstitial O atom in the lattice cell containing a vacancy introduces numerous small levels into the band gap and causes the shift and enhancement of degeneracy of small levels at the band gap edges. The obtained data shows that, unlike the single crystal silicon, the $Si_{28}VOH_{36}$ nanocluster doesn't have any deep level induced by the [V_{Si}-O_i] defect, which confirms that the deep level ($E_c - 2.186$ eV) in $Si_{28}OH_{36}$ is related to the interstitial O atom.

The calculation data shows that the C atom introduced in the $Si_{29}H_{36}$ nanocluster may occupy a main site and reduce the density of electron states at small levels at the band gap edges. When there is a vacancy in the C atom penetration area with formation of $Si_{27}VCH_{34}$, two H atoms are separated from the cluster. Considerable reduction of the density of electron states at the conduction band bottom is observed in this case both in $Si_{28}CsH_{36}$ and in $Si_{27}VCH_{34}$.

In case of simultaneous introduction of O and C atoms in the interstitial sites of the $Si_{29}H_{36}$, $Si_{28}VH_{36}$ nanoclusters, defect-induced energy band and level positions in the band gap as well as the densities of electron states vary considerably (Figure 5) and deep levels $E_{0\alpha} = E_c - 1.668\,\text{eV}$ and $E_{0\beta} = E_c - 4.126\,\text{eV}$ are formed in the $Si_{28}O_sC_iH_{36}$ cluster due to the bistable state of migrated H atoms and H atoms included in the 2H-C_i-V] complex. A [Si-O_i-V] defect complex is formed simultaneously, thus, preventing from formation of an oxygen-containing *A*-center. If one of the introduced atoms (O or C) occupies a main position during optimization, then deep levels $E_{0\alpha}$ and $E_{0\beta}$ induced by the formation of the [2H-C_i-V] and [Si-O_i-V] defect complex, disappear.

Increase in the nanocluster sizes with an increase in the content of Si atoms in the cluster drastically modifies the energy band positions near the $Si_{80}Si_{70}$ valence band ceiling. Small levels in this case merge into an intermediate band, and two deep levels ($E_V + 1.864\,\text{eV}$, $E_V + 2.128\,\text{eV}$) induced by the vacancy configuration are found in $Si_{86}VH_{70}$. Introduction of O and C atoms into interstitial sites of these nanoclusters drastically increases the densities of electron states in the defect formation area, thus, giving rise to a more energetically favorable [V_{Si}-Si_i] defect (Frenkel pair) and [O_i-2Si] defect without involvement of O_i and C_i. And the interstitial C forms equilibrium bonds with two Si atoms and contributes to the increase in the density of electron states throughout the nanocluster volume.

When O and C atoms are introduced in a lattice cell with large $Si_{86}VH_{70}$ nanocluster, the [O_i-V-C_i] defect complex turns to be more energetically and structurally stable in the formed $Si_{86}VO_iC_iH_{70}$ nanocluster, while the Frenkel pair is disintegrated, the density of electron states decreases a little at the valence band edge and increases at the conduction band edge. Energy band positions vary compared with small-size $Si_{28}O_iC_iH_{36}$, $Si_{27}VO_iC_iH_{36}$ nanoclusters. To determine the effect of large and small Si clusters, their energy properties were calculated.

Full internal bond energy of all atoms in the $Si_{29}H_{36}$ and $Si_{80}Si_{70}$ clusters is usually calculated with the density functional theory approximation and determined by the difference of full bond energies of the corresponding clusters with defects. Thus, the C and O formation energies are calculated as the difference of full energies of undoped ($E(Si_nH_m)$) and doped ($E(Si_{n-1}AH_m)$) structures using the following equation:

$$E_f = E(Si_{n-1}AH_m) - E(Si_nH_m) + \mu_{Si} - \mu_A \qquad (5)$$

where μ_{Si} is the full energy per a bulk Si atom, and μ_A is the full energy per an impurity atom (C or O). When both C and O atoms are present simultaneously, μ_A is the total full energy of the atoms (C + O). Calculated defect formation energies shown in Table 3 correspond to the assumption that the impurity atom in the Si clusters occupies a more energy favorable site in the lattice cell.

Comparison of the tabular bond energy data per each atom indicates high stability of the nanocluster electron structure containing O, C and V to the simultaneous formation of defect complexes.

A pronounced dependence of the charge and band gap distribution polarization on the size was found. Introduction of O and C impurity atoms into two neighboring lattice cells doesn't cause any changes of energy parameters, but increases the charge polarization drastically.

4. Findings and conclusion

Thus, the computer-based simulation results showed that process impurities in Si nanoclusters modified the band gap widths and defect formation energy, but this not always gave rise to deep levels in the band gap. It is shown that the change of sizes of a nanocluster containing Si_i atoms with simultaneous introduction of O and C gives rise to formation of weakly interacting defect complexes and H atom migration into the depth of the nanocluster. The density of electron states in the nanoclusters varies, the defect formation area symmetry decreases depending on the type of defect. It was found that, when an O atom is introduced into an interstitial site in the lattice cell, regardless of whether there is a vacancy V_{Si}, in the presence of an interstitial C impurity atom in the neighboring lattice cell, a Frenkel pair is formed and the cluster properties are not changed. It was found that deep levels might be caused by variation of the silicon cluster electron states due to the interaction between background impurities and a vacancy in the silicon cluster lattice cell. A H atom migration efficiency improvement mechanism was identified for small-size clusters containing impurity defects. ORCA computer-based simulation of three groups of $Si_{28}H_{36}:O$, $Si_{28}H_{36}:[V+O]$, $Si_{86}H_{70}:O$ and $Si_{85}H_{70}:[V+O]$; $Si_{28}H_{36}:C$, $Si_{28}H_{36}:[V+C]$, $Si_{86}H_{70}:C$ and $Si_{85}H_{70}:[V+C]$ and $Si_{28}H_{36}:O+C$, $Si_{28}H_{36}:[V+O+C]$, $Si_{86}H_{70}:O+C$ and $Si_{85}H_{70}:[V+O+C]$ clusters identified the dependence of O, CO + C atom positions on the nanocluster size and occurrence of the Jahn-Teller effect during interaction with the vacancy. This effect on the electron structure decreases as the nanocluster size increases.

Funding

The study was funded under the research and development program of the Nuclear Physics Institute of the Academy of Science of the Republic of Uzbekistan for 2020–2024.

Conflict of interest

The authors declare that they have no conflict of interest.

References

[1] M.G. Milvidsky, V.B Osvensky. Strukturnye defekty v monokristallakh poluprovodnikov. Metallurgiya, M. 1984, 256 s.: il.

[2] Voprosy radiatsionnoy technologii poluprovodnikov. Pod red. L.S. Smirnova. Novosibirsk, Nauka. 1980. s. 294. (in Russian).

[3] V.I. Fistul, Atomy legiruyushchikh primesey v poluprovodnikakh, M., Fizmatlit. 2004. S. 400. (in Russian).

[4] M.G. Mil'vidskii, V.V. Chaldyshev. FTP, **32**, 513 (1998). (in Russian).

[5] S.S.Nekrashevich, V.A.Gritsenko. FTT **56**, 209 (2014). (in Russian)

[6] D.A. Lozhkina, E.V. Astrova, R.V. Sokolov, D.A. Kirilenko, A.A. Levin, A.V. Parfenieva, V.P. Ulin. FTP, **55**, 373 (2021). (in Russian).

[7] I.F. Tchervony, A.V. Bubunets. Scientific J. „ScienceRice". **11**, *2*, 16 (2015).

[8] V.S. Vendamani, Hamad Syed, V. Saikiran, A.P. Pathak, S. Venugopal Rao, V.V. Ravi Kanth Kumar, S.V.S.J. Nageswara Rao. Mater. Sci. **50**, 1666–1672 (2015).

[9] K. Tokarska. Facile production of ultra-fine silicon nanoparticles. 2020 Facile production of ultra-fine silicon nanoparticles. R. Soc. Open Sci. **7**: 200736. (1–9). http://dx.doi.org/10.1098/rsos.200736

[10] H.M. Ayedh, E.V. Monakhov. J. Coutinho. Phys. Rev. Mater. **4**, 064601 (2020).

[11] M.Yu. Tamshetov, Sh.M. Mahkamov, F.T. Umarova, A.B. Normurodov, N.T. Sulaimanov, A.V. Khugaev, Kh.M. Kholmedov. FTP, **57**, *2*, 106–112 (2023). (in Russian). DOI:10.21883/FTP.2023.02.55330.3335

[12] Erik W. Draeger, C. Jeffrey. Grossman, Andrew J. Williamson, Giulia Galli. J. OF CHEM. PHYS., **120**, *22*, 10807–10814. (2004). [DOI: 10.1063/1.1738633]

[13] Frank Neese. Software update: the ORCA program system, version 4.0, 17 July 2017. // WIREs Computational Molecular sciences, Vol. 8, Issue 1, Jan./Febr. 2018, e1327. https://doi.org/10.1002/wcms.1327; F. Neese. The ORCA program system // Wiley Interdisciplinary Reviews: Computational Molecular Science. **2**, № 1. P. 73–78. (2012).

[14] G. Velde, F.M. Bickelhaupt, E.J. Baerends, C. Fonseca Guerra, S.J.A. van Gisbergen, J.G. Sijders, T. Ziegler. J. Comp. Chem. **22**, 931 (2001).

[15] F. Weigend, R. Ahlrichs. Balanced Basis Sets of Split Valence, Triple Zeta Valence and Quadruple Zeta Valence Quality for H to Rn: Design and Assessment of Accuracy. Phys. Chem. Chem. Phys., **7**, 3297–3305 (2005). https://doi.org/10.1039/b508541a.

[16] G. Velde, F.M. Bickelhaupt, E.J. Baerends, C. Fonseca Guerra, S.J.A. van Gisbergen, J.G. Sijders, T. Ziegler. J. Comp. Chem. **22**, 931 (2001).

[17] E. Van Lenthe, E.J. Baerends. J. Comp. Chem. **24**, 1142 (2003).

[18] Sh. Makhkamov, F.T. Umarova, A.B. Normurodov, N.T. Sulaymanov, O.B. Ismailova. Uzbek. Phys. J. **18**, 82 (2016).

[19] L.I. Murin, B.G. Svensson, J.L. Lindströ m, V.P. Markevich and C.A. Londos. Solid State Phenomena. **156–158**, 129–134 (2010).

[20] International Tables for Crystallography. Volume A: Space-group symmetry / Edited by M.I. Aroyo. — International Union of Crystallography, 2016 — ISBN 978-0-470-97423-0. (https://it.iucr.org/A c/)

[21] V.M. Babich, N.I. Bletskan, E.F. Venger. Kislorod v monokristallakh kremniya Kiev. InterpresLTD, 1997. 240 s. (in Russian).

[22] A.A. Gnidenko, V.G. Zavodinsky. FTP, **42** (7), 817–822 (2008). (in Russian).

[23] V.V. Lukjanitsa. Semiconductors, **37**, *4*, 404–413 (2003) Translated from Fizika i Tekhnika Poluprovodnikov, **37**, *4*, 422–431 (2003).

[24] G.D. Wotkins, K.L. Brower. Phys. Rev. Lett., **36**, 1329 (1976). DOI: https://doi.org/10.1103/PhysRevLett.36.1329

[25] Noura D. Alkhaldi, Sajib K. Barman, Muhammad N. Huda. Heliyon. **5**, *11*, e02908 (2019).

[26] P.A. Selishchev. Semiconductors, **35**, *1*, 11–14 (2001).

[27] V.K. Lyuev, A.M. Karmokov. Sovremennye naukoemkie tekhnologii, **5***2*, 262–265 (2016). (in Russian).

[28] Silicon Nanocrystals: Fundamentals, Synthesis and Applications. Edited by Lorenzo Pavesi and RasitTuran — 2010 WILEY-VCH Verlag GmbH & Co. KGaA, Weinheim, P. 652. ISBN: 978-3-527-32160-5.

[29] C.A. Londos and J. Grammatjkak. Phys. Stat. Sol. (a) **109**, 421–426 (1988).

[30] Z.M. Khakimov, F.T. Umarova, N.T. Sulaymonov, A.E. Kiv, A.A. Levin. Int. J. Quantum Chem. **93**, *5*, 351–359 (2003).

Translated by E.Ilinskaya